PAPER • OPEN ACCESS

Triboelectric proximity and contact detection using soft planar spiral electrodes

View the article online for updates and enhancements.

Triboelectric proximity and contact detection using soft planar spiral electrodes

L E Helseth

Department of Physics and Technology, Allegaten 55, NO-5020 Bergen, University of Bergen, Norway

E-mail: Lars.Helseth@ift.uib.no

CrossMark

Abstract

In this study, planar spiral electrodes for triboelectric contact and proximity detection are investigated. The spiral electrodes are created using liquid metal in a soft elastomer in order to make the sensor flexible and stretchable. When the metallic object to be detected comes in contact with the silicon elastomer surrounding the electrodes, charge transfer occurs, and this can be utilized for contact and noncontact sensing of the metallic object in flat or curved geometries. An equivalent electrical circuit model for the noncontact system is proposed and found to be in good agreement with the experimental data. A comparison between triboelectric proximity detection and eddy current resonance frequency proximity detection, using the same electrode geometry, shows that the two methods have comparable sensitivity. An added advantage of the triboelectric system is that it transforms mechanical into electrical energy and thereby allows one to monitor the triboelectrical signal upon impact of a metal object, and the experimental data show that the generated current scales with the impact force.

Keywords: triboelectric, proximity sensing, elastomer

(Some figures may appear in colour only in the online journal)

1. Introduction

Triboelectric nanogenerators have attracted considerable interest due to their ability to convert mechanical energy from the surroundings into electrical energy [1, 2]. Triboelectric nanogenerators can generate electrical energy through vertical, sliding or other modes with different electrode geometries [2–5], surface roughness [6–9] and nanoparticle composites [10]. Creative design allows one to include them wireless transmission systems [11], security systems [12], as energy harvesters in shoes [13], clothes [14–16] or smart skin [17–20]. Triboelectric nanogenerators have also been demonstrated to be useful for creating vibration [21], touch [22] and noncontact motion sensors [23]. Soft and stretchable triboelectric generators can be fabricated by embedding electrodes in the form of liquid metals [24, 25] or silver flakes [20] in a silicone elastomer matrix. The unique ability of

liquid metals to change shape without local buildup of stress make them very useful for soft electronics, where the design and printing of circuit components is done directly in air or encapsulated in elastomers. On the other hand, metal films may crack or deform when stressed, such that the electrical resistance changes and thus alter the performance of the triboelectric generator. Similarly, other solid materials such as conducting particles in a carrier liquid may contribute to local stress when the soft device is being stretched or bent, thus altering the electrical output parameters.

In the current study, soft planar spiral electrodes for triboelectric contact and noncontact sensing of the metallic objects are being studied. While such planar electrodes have been studied for use in induction and eddy current sensing [26–28], less is known about their performance when triboelectrically induced charges are used for contact and noncontact sensing. Research has demonstrated that systems based on cylindrical spiral or hybrid triboelectric and electromagnetic generators can be based on three-dimensional spiral geometries [29, 30], but planar spiral geometries based on strain-absorbing soft materials for use in human devices have not been investigated. It is known that the electrodes
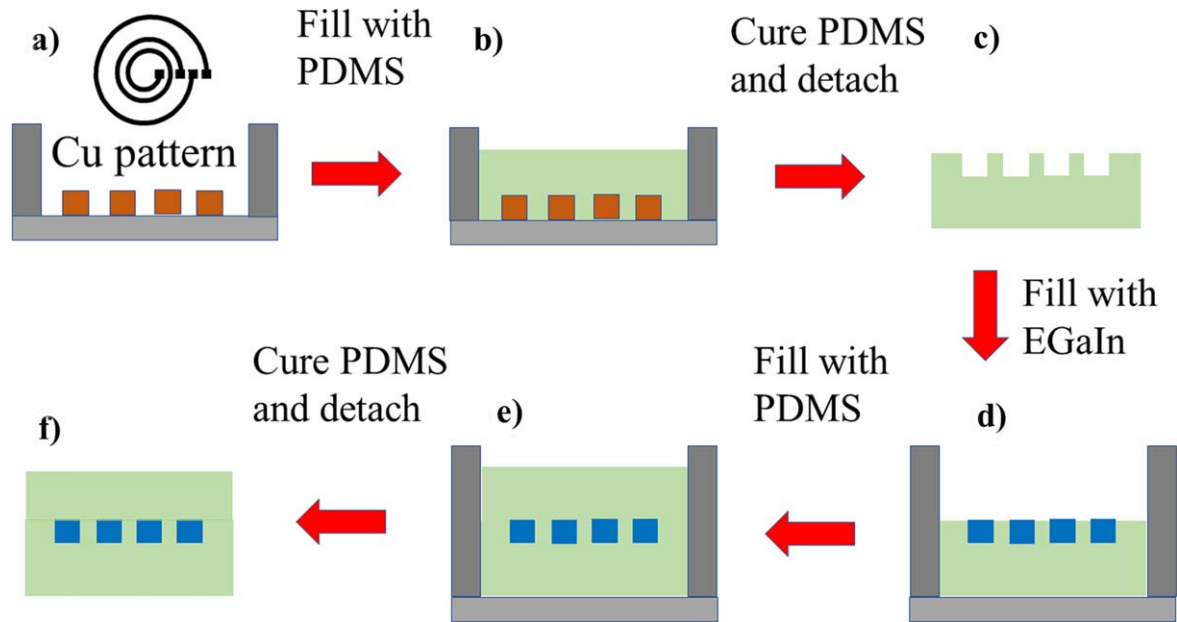
Figure 1. Schematic diagram showing how the elastomer-embedded liquid metals electrodes are created. First, copper pattern is created using a spiral photomask and standard ultraviolet lithography on photoresist followed by development and etching (a). The copper pattern is covered with liquid elastomer (b), which is subsequently cured and removed from the copper pattern(c). The liquid EGaIn metal alloy is filled into the trenches (d), and liquid elastomer covers the EGaIn (e) before it is cured (f).

involved triboelectric systems often determine the performance of the device, and parasitic capacitances have to be taken into account [31]. In the current study, an equivalent electrical circuit model for the noncontact system taking into account capacitive couplings is found to explain the experimental data quantitatively. A comparison shows that the triboelectric proximity detection performs comparably to an eddy current resonance frequency detection system utilizing the same spiral electrode geometry. In addition, the triboelectric sensor system exhibits a force-dependent impact signal when metallic objects come into contact with the elastomer, thus allowing contact sensing more precisely than an eddy current sensor.

2. Materials and methods

The elastomer-embedded liquid metal coils are created as demonstrated in figure 1. First, standard lithography is used to create $100\,\mu\text{m}$ thick copper pattern on a standard epoxy substrate (figure 1(a)). The copper pattern consists of two spiral electrodes, which were designed and developed using ultraviolet lithography and chemical etching. The copper track has a width 2.9 mm, and there is a gap of 3.1 mm between the tracks. The outer spiral electrode has an inner radius 50 mm and is designed for excitation of the MHz electromagnetic radiation or for leading current to ground when used as triboelectric generator.

The inner spiral electrode is designed for detection, i.e. either for detecting the MHz electromagnetic radiation or for collecting the current that is generated upon triboelectric generation. The latter has 2 turns, has inner diameter 14 mm and outer diameter of 37 mm, and can be represented by an

Archimedean spiral with radius $r = 0.9\theta$ (in millimeter), where θ is the angle. The selection of this particular geometry was a compromise between the requirements of an eddy current sensor and that of a triboelectric generator to allow one to investigate the two principles independently with the same geometry. The application as a triboelectric nanogenerator required a flexible electrode geometry that generate current while at the same time could be fitted on a normal arm to keep the system reasonably small. These concerns restricted the inner diameter of the outer electrode to about 50 mm. Smaller diameters would result in reduced signal from the inner electrode, thus leaving the given geometrical parameters as a good choice.

After fabricating the copper mask, it is surrounded by foam tape which acts as barriers when the liquid elastomer is poured on top of the mask (figure 1(b)). Here we used two-component Sylgaard 184 of 10:1 elastomer to curing agent ratio, which is degassed in vacuum until no bubbles are observed. The bubble-free liquid is cured at 110 °C for 30 min, and the cured polydimethylsiloxane (PDMS) is peeled off the mask (figure 1(c)). Next, EGaIn is deposited in the channels using a pipette (figure 1(d)). To avoid spill and to keep the area outside the grooves as clean as possible, a cotton swab is dipped in NaOH solution (1 M) and moved over the elevated regions. Since NaOH is known to remove the oxide layer of the liquid EGaIn, any liquid metal residue coming in contact with NaOH will form small spheres that can easily be removed. The liquid metal residing in the grooves is covered by liquid PDMS (figure 1(e)), which is subsequently cured and the whole device is detached from the substrate (figure 1(f)). The total thickness of the elastomer is about 1 mm, and the thickness of the liquid metal conducting traces is about $100\,\mu\text{m}$. An example of one of the flexible
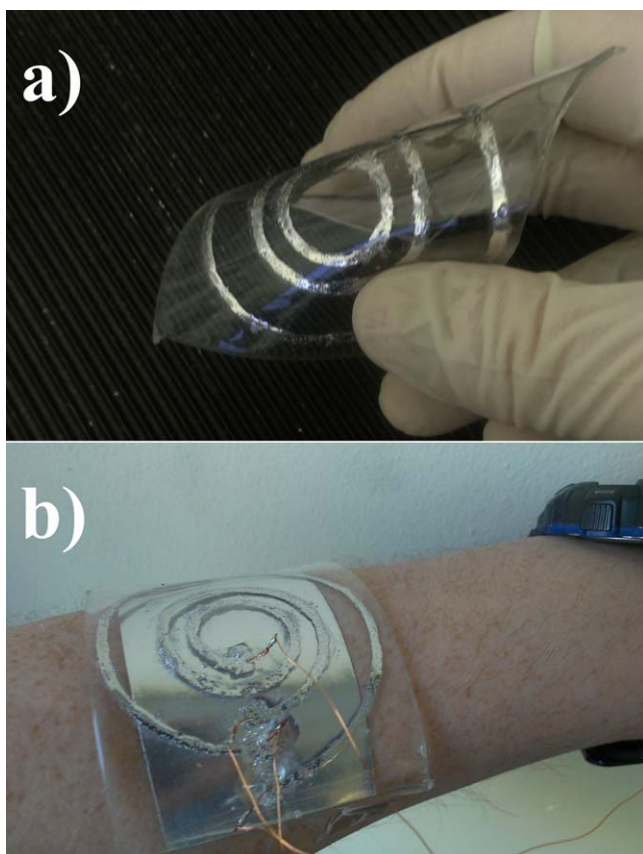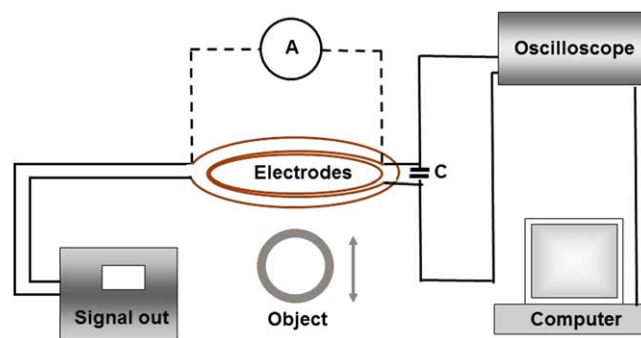
Figure 2. Pictures of spiral electrodes. In (a), a 1 mm thick elastomer-embedded liquid metal coil system are depicted after curing the PDMS. In (b), the elastomer-embedded liquid metal electrode system is mounted on an arm for detection of a metal film.


Figure 3. Experimental setup. For eddy current resonance frequency proximity detection, a signal generator feeds a broadband pulsed signal into the larger liquid metal spiral electrode. The smaller liquid metal spiral electrode is connected in parallel with an external capacitor, and the detected signal recorded by a computer controlled oscilloscope. The elastomer embedding the electrodes are not shown. When measuring the triboelectric signal, the capacitor C, the signal generator and the oscilloscope are disconnected, and the current (or voltage) is measured over the electrodes shown as dashed lines.

spiral electrodes of thickness 1 mm fabricated in this way is shown in figure 2(a).

Solid metal wires were connected to the liquid metal spiral electrodes. The simplest method used here was to penetrate the PDMS with small pieces of 0.4 mm copper wire, such that the copper makes direct contact with the EGaIn. The 0.4 mm copper wire is stiff enough to easily penetrate the PDMS, and is welded to even thinner (0.1 mm), but longer (typically about 15 cm) copper wire to ensure flexibility. As an alternative connection between the EGaIn and solid metal wires, short 0.4 mm polymer-covered copper wires were directly welded to BNC contacts. Unfortunately, the stiff copper wire would, upon bending, easily create cracks in the thin elastomer were liquid metal could leak out. To avoid this, an extra thick elastomer (thickness 2.5 mm) could be used, containing an additional layer of PDMS near the connection points to avoid cracks. This increased thickness (2.5 mm) came at the cost of reduced flexibility as compared to the thinner elastomer substrates (0.5–1 mm). For this reason, thinner wires like those seen in figure 2(b) were preferred.

The electrodes can be used in two different modes independently, either for detection of objects using the triboelectric detection principle or eddy current resonance frequency proximity detection. See figure 3. When using the system as a triboelectric generator, the signal generator and

the oscilloscope were disconnected, and the generated current or voltage was measured using a Keithley 6514.

When monitoring the presence of metal samples using resonance eddy current detection, the thin copper wire on the outer excitation electrode is connected through a BNC-contact directly to a signal generator, see figure 3. The signal generator, TTi TG200, generates a voltage pulse of 10 V of rise time about 30 ns, thus generating a broadband magnetic field near the detection electrode. The ends of the copper wire connected to the inner detection coil are coupled to a BNC contact which is coupled in parallel with a polyester foil capacitor of capacitance $C = 2.7 \pm 0.1$ nF. This was capacitor was selected to force the system into a suitable resonance to facilitate easier eddy current detection, see [27] for explanation of the principle. The reason for selecting an external polyester foil capacitor, and not an elastomer-embedded liquid metal capacitor, was that the latter only allows relatively small capacitances using the selected fabrication method (typically smaller than 100 pF), which would create a too large resonance frequency and too high sensitivity towards unwanted stray capacitances for sensitive eddy current detection using the setup considered here. The signal was read out by a digital oscilloscope (PicoScope 5204) set at a sampling frequency of 1 GHz.

3. Triboelectric proximity sensing

When the elastomer is brought in contact with the metallic object under study, contact electrification occurs. If the PDMS is brought in contact periodically with a flat metal piece of the same size as the elastomer, under an applied force of peak 5 N, one obtains a peak current of nearly 4 μA as seen in figure 4(a). The charge transfer during one contact event was calculated by integrating the current of one single pulse in figure 4(a) according to $\int I dt$. Doing this for all the pulses
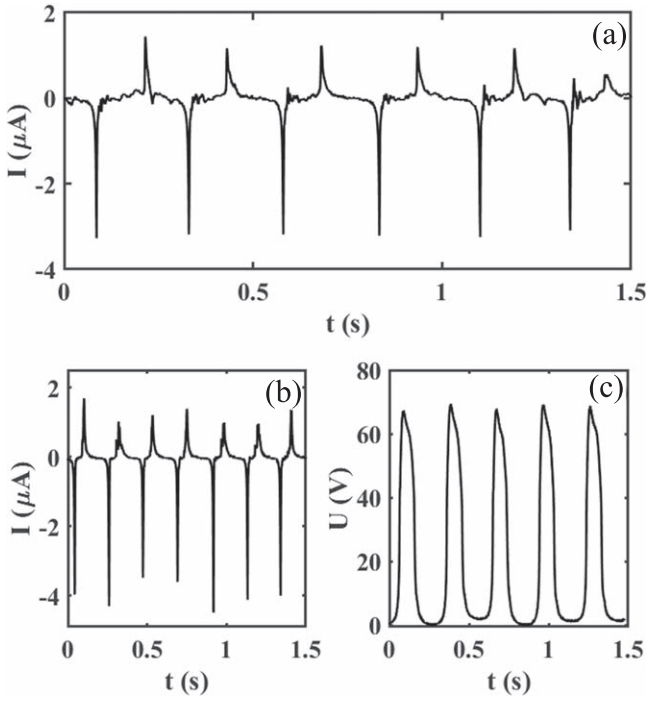
Figure 4. The current measured running from the inner to the outer liquid metal electrode when a flat (a) or a curved (b) metal surface is contacting the elastomer with a force of about 5 N. Also shown is a graph of the open circuit voltage when the curved metal surface was contacting the elastomer (c).

in figure 4(a) and then taking the average, it is seen that the charge transfer is of the order of 20 nC.

The peak current remains nearly the same if the PDMS is brought periodically in contact with a curved metal film of diameter 40 mm, see figure 4(b). The open circuit voltage may exceed 60 V as seen in figure 4(c).

The working mechanism of the triboelectric generator is the freestanding triboelectric layer mode (see [2, 21, 23]), since the metallic object is located above the dielectric (PDMS) encapsulating the liquid metal electrodes. However, we note one additional novelty of the current setup. Since the electrodes are asymmetric, i.e. the inner and the outer electrodes cover different areas, there is an additional charge transfer, which explains why the currents in figure 4(a) are larger than those found for interdigitated electrodes made of the same elastomer and liquid metal combination (see [25]). Due to the asymmetry in the electrode geometry, additional charge transfer occurs when the object approaches.

The triboelectric charge formed upon contact between metal and PDMS remains even after the metal is removed for hours. If the metal film is placed in proximity of the encapsulated liquid metal electrode, the induced charge increases as the metal approaches. Setting the flat metal film into oscillations at a frequency of 6 Hz and amplitude about 1 cm, a current will be induced between the inner and outer spiral electrodes. This is illustrated in figure 5(a), where the closest distance z (during oscillations) between metal and PDMS is 3 mm (left side) or 25 mm (right side). The induced peak current I_p decreases as the closest distance z between the metal and elastomer changes, as seen in figure 5(b).

The observed behavior in figure 5(b) can be explained by considering the electrostatics of the system. The PDMS and liquid metal electrodes have initially no net charge. When the copper plate is brought in contact with the PDMS, a charge $-Q$ is transferred to the isolator and $+Q$ to the metal due to the triboelectric effect. The charges $+Q$ and $-Q$ form a double layer that maintains neutrality, since the net charge is assumed to be zero. When the copper plate is separated from the PDMS, the charges in the double layer are separated. If unequal amount of charge is formed in the two spiral liquid metal electrodes, charge may flow from one electrode to another. To model the process, an equivalent electrical circuit for the system is shown in figure 5(c). Here C_{12} is the capacitance between the two electrodes. C_{air}^1 is the capacitance associated with the layer of tribocharge on the PDMS surface right above the inner spiral electrode surface and the copper plate located in air. Similarly, C_{air}^2 is the capacitance associated with the layer of tribocharge on the PDMS surface right above the outer spiral electrode surface and the copper plate located in air. The areas of the inner and outer electrodes are A_1 and A_2, respectively, and if one make the approximation of plane-parallel capacitors one may set $C_{air}^1(t) \approx \varepsilon_0 A_1/z(t)$ and $C_{air}^2(t) \approx \varepsilon_0 A_2/z(t)$. Here ε_0 is permittivity of air and $z(t)$ is the distance between metal and PDMS. Since A_1 and A_2 are comparable, it is seen that the equivalent capacitance between the electrodes and the copper plate is $C_{air} = C_{air}^1 C_{air}^2/(C_{air}^1 + C_{air}^2) \approx C_{air}^1/2$. Equivalently, one may write $C_{air}(t) \approx \varepsilon_0 A/z(t)$, where $A \approx A_1/2$. The capacitance between the PDMS surface and the inner and outer spiral electrodes are C_{iso}^1 and C_{iso}^2, respectively. Since the distance between the copper plate and the liquid metal electrodes is always fulfilling $z \gg d/\varepsilon$, where $\varepsilon = 2.7$ is the relative permittivity of PDMS [32, 33] and $d = 0.5$ mm is the thickness of PDMS separating liquid metal from air, we may assume that the corresponding voltages associated with C_{iso}^1 and C_{iso}^2 are negligible. A charge $-q$ is now located in the copper plate, and this charge compensates a fraction of the $Q_1 - q$ charges on the surface of the PDMS.

The voltage difference between the inner and outer spiral electrodes is now given by

$$V(t) = \frac{Q_1 - q}{C_{12}} - \frac{q}{C_{air}} \approx \frac{Q_1 - q}{\varepsilon_0 \varepsilon A_{12}} w - \frac{q}{\varepsilon_0 A} z(t), \quad (1)$$

where the latter expression assumes that the spiral electrodes can be approximated by plane-parallel capacitors with capacitance $C_{12} = \varepsilon_0 \varepsilon A_{12}/w$, where A_{12} is the part of the area of the inner electrode towards the outer electrode and w the distance between the inner and outer electrodes. The current through the resistor R is given by $I = dq/dt = V(t)/R$, or

$$I(t) = \frac{Q_1}{RC_{12}} - \frac{q}{R}\left(\frac{1}{C_{air}^1} + \frac{1}{C_{12}}\right). \quad (2)$$

We assume short circuit conditions, which means that $V(t) = 0$ (or equivalently, $R = 0$), such that the potential at the two metal electrodes remains the same. Then equation (2) can
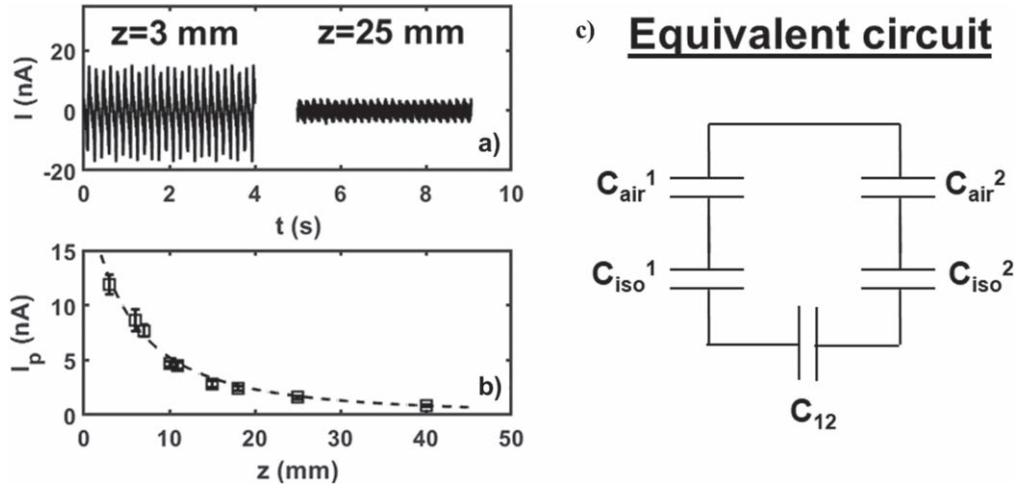
Figure 5. The current measured running from the inner to the outer electrodes when a flat metal surface is moving back and forth at a frequency 6 Hz and amplitude of about 1 cm (a). The smallest distance from the metal plane is $z = 3$ mm (larger oscillations on the left side) or $z = 25$ mm (smaller oscillations on the right side). The peak current I_p as a function of distance z (b). In (c) an electrical equivalent circuit for the triboelectric spiral electrode system is shown.

be transformed into

$$q(t) \approx \frac{Q_1}{1 + \frac{C_{12}}{C_{air}^1}} = \frac{Q_1 w A}{A_{12} \varepsilon} \frac{1}{z(t) + \frac{w}{\varepsilon} \frac{A}{A_{12}}}. \quad (3)$$

The short-circuit current when $z(t)$ is changing is given by

$$I_{sh} = \frac{dq(t)}{dt} \approx -Q_1 \frac{u w A_1}{A_{12} \varepsilon} \frac{1}{\left(z(t) + \frac{w}{\varepsilon} \frac{A}{A_{12}}\right)^2}, \quad (4)$$

where $u = dz/dt$ is the velocity of the copper plate relative to the liquid metal electrodes. Figure 5(b) shows a fit of equation (4) to the experimental data with $a = Q_1 u w A_1/(\varepsilon A_{12}) = 2.1 \times 10^{-12}$ Am^2 and $b = w A_1/(\varepsilon A_{12}) = 1.0 \times 10^{-2}$ m. Since the plane-parallel approximation used here is rather rough, the effective area A_{12} is not known precisely. One might expect that only the outer part of the inner electrode interacts efficiently with the outer electrode, in which case one may expect A/A_{12} to be in the range between 1 and 2. Moreover, the distance between the outer and inner electrodes is $w \approx 13$ mm, which means that one can estimate an upper value $b = w A_1/(\varepsilon A_{12}) \approx 10^{-2}$ m, in agreement with the fit of equation (4) to the experimental data. From the fit of equation (4) to the experimental data one also obtains $u Q_1 = 2 \times 10^{-9}$ Am, which means that $Q_1 \approx 5 \times 10^{-9}$ C since $u \approx 0.4$ m s^{-1}. This is only one quarter of the total charge of 20 nC transferred during touch as found from figure 4. It is likely that some of the contact charge transferred during contact with the flat copper plate either does not remain on the PDMS surface or does not participate in the charge transfer due to some loss of electrostatic coupling when the copper plate is moved away from the polymer. It is also known that the triboelectric charge on the surface of polymers gradually becomes neutralized by the presence of water molecules and other molecules existing in the humid air. In our system, the charge decay is not fast and is observed to decay slowly over the time span of one day. Thus, any experiment that could be finished within one hour would not suffer from charge losses. Moreover, it is

possible to recharge the surface by contacting it with metal. On the other hand, if the charge must remain stable over hours while performing an experiment, the whole system must be put in vacuum. However, this is outside the scope of the current work.

4. Eddy current proximity sensing

An eddy current proximity sensing using the excitation and detection scheme illustrated in figure 3 was set up to assess the proximity detection performance of the new triboelectric sensing system. The electrodes had the same geometry as reported above. Figure 6 shows the voltage signal in time domain (a) and frequency domain (b) picked up by the inner electrode which is connected in parallel with an external capacitor $C = 2.7 \pm 0.1$ nF.

The signal measured by the oscilloscope is on the form $V(t \leqslant 0) = 0$ and

$$V(t) = V_0 e^{-t/\tau} \sin(2\pi f_R t), \quad t \geqslant 0, \quad (5)$$

where V_0 is the peak signal, f_R the resonance frequency and τ is the decay time. In principle, all three parameters, V_0, f_R and τ can be used to detect metals due to the setup of eddy currents in these. However, it was found that the peak signal V_0 and the resonance frequency f_R were the most stable and reproducible parameters in the available system. The method for identifying the resonance frequency is based on performing a nonlinear fit of a lorentzian curve

$$S(f) = \frac{S_A}{(f - f_R)^2 + \frac{1}{(2\pi\tau)^2}}, \quad (6)$$

to the experimental data. Here S_A is a constant which in practice is set numerically such that the spectrum is normalized. In figure 6(b) a fit of equation (6) is shown with $f_R = 5.43 \pm 0.01$ MHz as the resonance frequency and $\tau = 1.86 \pm 0.01$ μs as the decay time. While the single measurement precision is good, repetition of the experiments
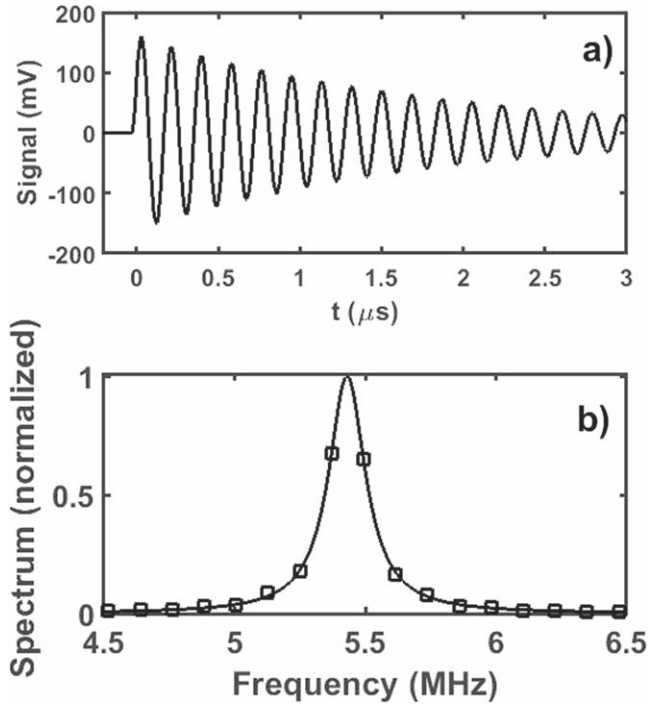
Figure 6. The signal detected by the (smaller) detection spiral electrode (a) and the corresponding frequency spectrum (b). The solid line in (b) is a fit of a lorentzian curve to the experimental data.

shows larger variations, particularly in the time constant. The loss factor is small since the measured resistance in the excitation coil $R < 1\,\Omega$ was measured for the situations studied, $(R/L)^2 \ll 1/LC$, and the resonance frequency can be approximated by $f_R = 1/2\pi\sqrt{LC}$. That is, the resistance of the liquid metal electrode does not play a significant role here. While the capacitance of the system is mainly governed by the external capacitor, the inductance can be estimated using the resonance frequency to be $L \approx 1/(2\pi)^2 f_R^2 C \approx 0.3\,\mu H$. Using equation (2) of [28] one obtains $0.1\,\mu H$, which is of comparable magnitude. The deviation of the observed and estimated inductances can be attributed to the wires used to connect the coaxial cables with the excitation electrode. Since the skin effect influences the performance of eddy current detections, one should be aware of this parameter when designing the systems. At a given frequency f, the skin depth can be estimated using $1/\sqrt{\pi\mu_m\sigma f}$, where μ_m is the permeability. At $f = 5\,MHz$, the skin depth is $122\,\mu m$ for EGaIn, which is larger than the thickness of the liquid metal. Thus, the electromagnetic field fully penetrates the conducting tracks at the considered frequencies, such that the sensitivity is not influenced by variations in frequency slightly above or below the used frequency.

Figure 7(a) shows the signal when the elastomer with embedded liquid metal coils is in close contact with a 0.1 mm thin aluminum film either in a flat state (red curve), or a curved state (blue curve). The diameter of the curved metal film was 40 mm. Curling the coil around the metallic object brings the spiral electrodes in closer contact, thus increasing the eddy currents (in the object) and subsequently reducing

the measured signal in the inner spiral electrode. The voltage amplitude and the resonance frequency were recorded as a function of position, where the elastomer containing liquid metal remained curved with a diameter of 40 mm at all times. This was done by holding the elastomer in place by small polymer grips (which were found not to influence the signal or resonance frequency) such that it remained fixed in a curved state. Figure 7(b) shows the peak voltage, whereas figure 7(c) shows the resonance frequency as a function of position.

The change in resonance frequency with the presence of metal seen in figure 7(c) can be modeled using Bethe–Schwinger perturbation theory, which gives [27, 34, 35]

$$f_R = \frac{f_0}{1 + \beta(\sigma, \mu_m, d)}, \tag{7}$$

where $\beta(\sigma, \mu_m, d)$ is a complex function of the conductivity σ of the sample, the permeability μ_m of the sample and the distance d. As in [27], this function can be well approximated by $\beta(\sigma, \mu_m, d) = -a(\sigma, \mu_m) \exp(-d/d_0)$, where $a(\sigma, \mu_m)$ and d_0 are fitting parameters. The solid line of figure 7(c) is a fit of equation (7) to the experimental data using $f_0 = 5.8\,MHz$, $a = -0.10$ and $d_0 = 3.3\,mm$.

At small distances z, the resonance frequency can be monitored at a sensitivity $0.2 \pm 0.1\,MHz\,mm^{-1}$ using eddy current resonance frequency proximity detection. In the same distance range, the voltage amplitude can be detected with a sensitivity of $13 \pm 5\,mV\,mm^{-1}$. However, this amplitude is easily disturbed by external radio sources, and it turns out that the resonance frequency can be monitored more accurately in the long run. On the other hand, the triboelectric signal can be monitored at a sensitivity of $1.1 \pm 0.7\,nA\,mm^{-1}$ as in figure 5(b). While this signal is also possible to influence by other metallic or dielectric objects, it turns out to be more robust towards influence of for example external radio signals than the amplitude voltage obtained in the eddy current scheme. Thus, these widely different methods are comparable in terms of relative sensitivity and provide detection schemes that may complement each other.

5. Triboelectric impact sensing

One particular advantage of the sensor system presented here is the flexibility and stretchability of the spiral electrodes, which allows one to monitor the triboelectric signal upon impact of curved metallic objects. In figure 8(a) a steel ball of diameter 25 mm is pressed against the elastomer containing liquid metal electrodes. When the steel ball is pressed periodically against the elastomer with a force of 5 N, the measured current (figure 8(b) and voltage (figure 8(c) vary with time. It is noted that the peak current, voltage and also the total induced charge in the external wires is considerably less than observed for an extended flat or curved metal plate as was reported in figure 4, simply due to the fact that the steel ball has a diameter smaller than the inner liquid metal electrode such that the electrostatic coupling is smaller.
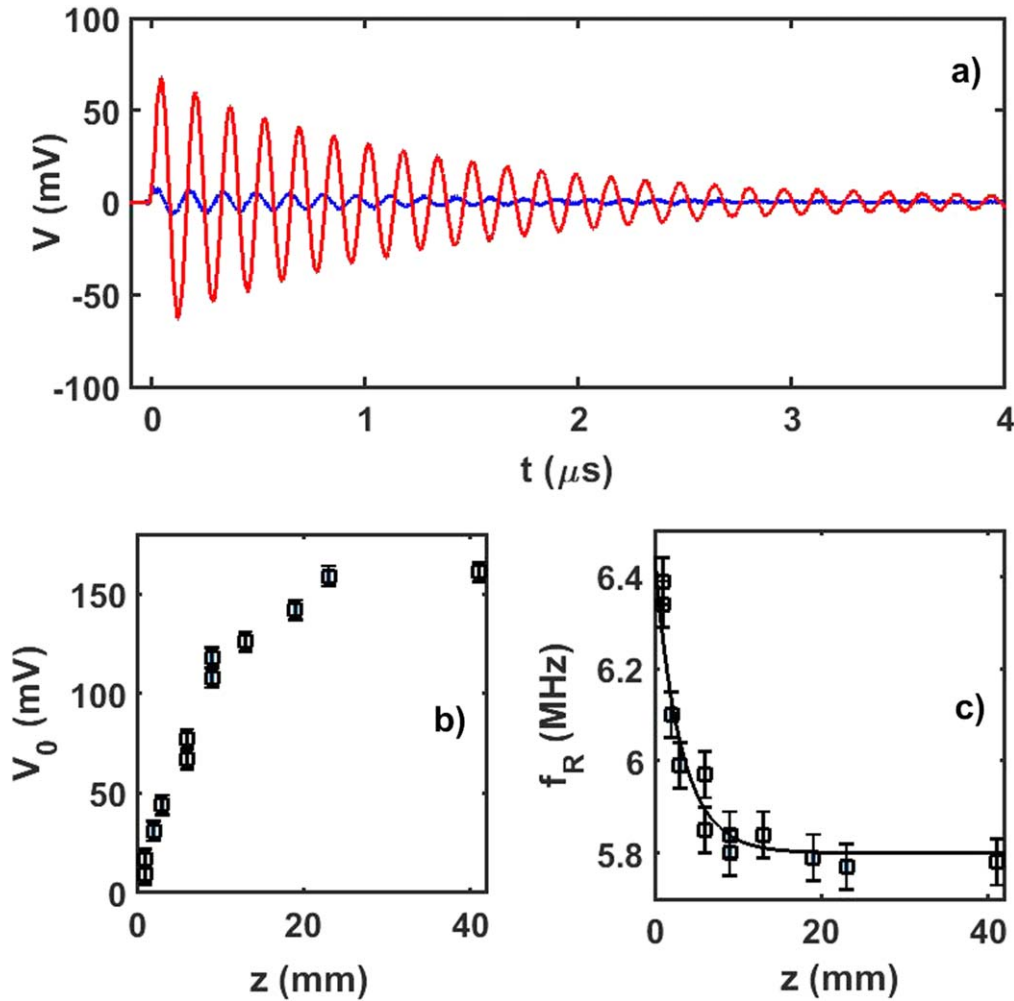
Figure 7. The flat (red) and the curved (blue) elastomer-embedded liquid metal spiral electrodes placed in vicinity of cylindrical aluminum film of 40 mm diameter (a). The peak signal (b) and resonance frequency (c) for a curved spiral electrode system as a function of distance to the curved aluminum film.

The peak current increases with increasing peak force as seen in figure 8(d), although there are large statistical variations. Theoretically, one may obtain some insight by assuming that the charge is given by $Q_b = \sigma A$, where σ is the triboelectrically induced surface charge density and A is the contact area between the steel ball and the elastomer. Both these variables are in general time-dependent, but some insight can be obtained by assuming that the charge density is constant. One may then write the current as $I_b = \sigma dA/dt$, where the rate dA/dt is approximately the same for every force applied, and could be given by $A = A_{pf}f(t)$, where $f(t)$ is some periodic function and A_{pf} is the maximum contact area between metal and PDMS. The peak current is therefore expected to be proportional to the maximum contact area, i.e. $I_b \propto A_p$. Previous studies have demonstrated that the triboelectric signal scales with force [36]. In Hertz' contact theory between a sphere and an elastic half-space, the contact area is related to the applied force through a power law, i.e. $A_p \propto F^{2/3}$, and one therefore expects that the peak current should grow proportionally to $F^{2/3}$. The large variations in the peak current, and therefore also the transferred

triboelectric charge, seen in figure 8(d), means that it is difficult to attribute a specific power law that relates the peak current and applied force. These variations are most likely related to variations in the surface charge density as one stretches the elastomer, as it is known that surface stress influences the surface charge. However, one does observe from figure 8(d) that the peak current increases with applied force, in qualitative agreement with the arguments above. It is also seen that the peak current in figure 8(d) is significantly larger than that of figure 5(a), but smaller than that of figure 4(b). This is due to the fact that the steel sphere only comes in contact with a limited area of the elastomer, inside the region of the inner spiral electrode (i.e. 14 mm). There is no direct contact between the steel ball and the dielectric elastomer directly above the position of the inner electrode, such that all induced charge is due to the capacitive coupling through air. On the other hand, when there is no contact at all (as in figure 5), the induced charges in the liquid metal are significantly smaller than those observed during contact, thus allowing one to distinguish contact and noncontact by observing the peak current.
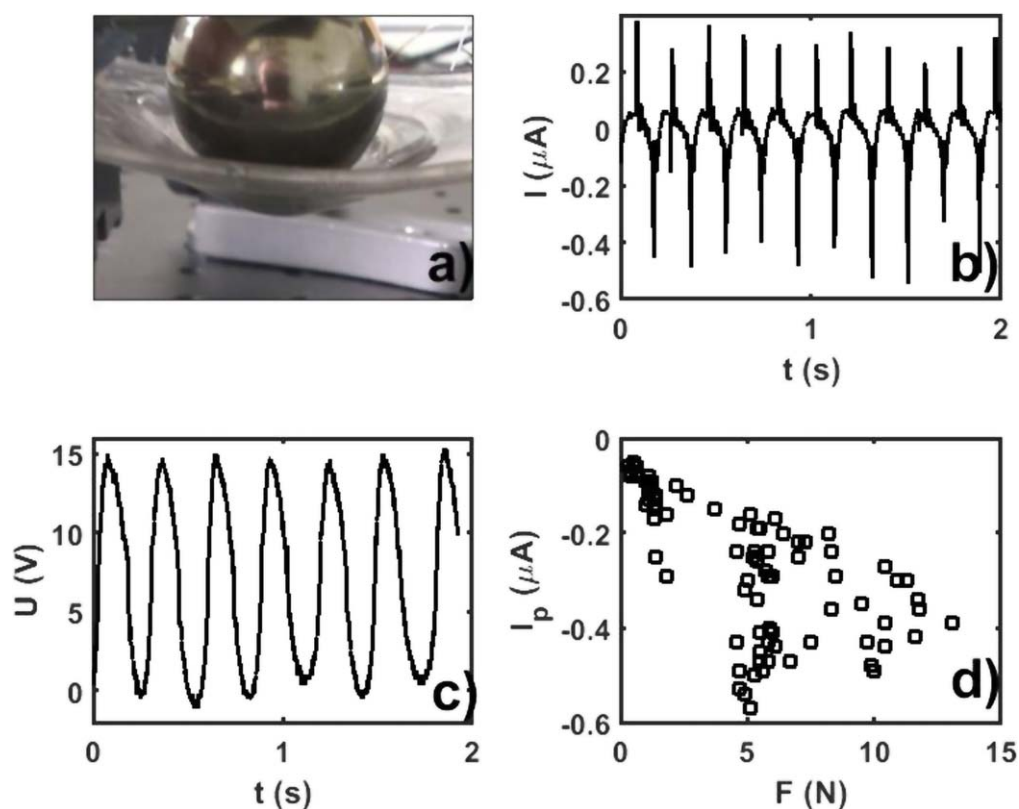
Figure 8. A steel ball of diameter 25 mm is pressed against the elastomer containing liquid metal electrodes (a). When the steel ball is pressed periodically against the elastomer with a force of 5 N, the measured current (b) and voltage (c) varies with time. The peak current increases with increasing peak force (d).

6. Conclusion

In this study, it has been demonstrated that spiral electrodes in an elastomer can be used to detect proximity and contact with a metal in flat or curved shape using triboelectric charges. An equivalent electrical circuit model for the noncontact tribo-electric system is proposed and found to be in good agreement with the experimental data. Such planar, spiral triboelectric detection systems have merits as self-powered detection systems, and have here been shown to compare well with a resonance frequency eddy current detection scheme that requires power to work.

ORCID iDs

L E Helseth https://orcid.org/0000-0002-2685-3744

References

[1] Fan F R, Tian Z Q and Wang Z L 2012 Flexible triboelectric generator *Nano Energy* **1** 328–34
[2] Wang S, Lin L, Xie Y, Jing Q, Niu S and Wang Z L 2013 Sliding-triboelectric nanogenerators based on in-plane charge-separation mechanism *Nano Lett.* **13** 2226–33
[3] Wang Z L, Lin L, Chen J, Niu S and Zi Y 2016 *Triboelectric Nanogenerators* (Switzerland: Springer)
[4] Liu W, Han M, Sun X, Meng B, Zhang X S and Zhang H X 2014 An unmovable single-layer triboelectric generator driven by sliding friction *Nano Energy* **9** 401–7
[5] Guo X D and Helseth L E 2015 Optical and wetting properties of nanostructured fluorinated ethylene propylene changed by mechanical deformation and its application in triboelectric nanogenerators *Mater. Res. Express* **2** 015302
[6] Zhao L, Zheng Q, Ouyang H, Li H, Yan L, Shi B and Li Z 2016 A size-unlimited surface microstructure modification method for achieving high performance triboelectric nanogenerators *Nano Energy* **28** 172–8
[7] Rasel M S and Park J Y 2017 A sandpaper assisted micro-structured polydimethylsiloxane fabrication for human skin based triboelectric energy harvesting application *Appl. Energy* **206** 150–8
[8] Nafari A and Sodano H A 2018 Surface morphology effects in a vibration bases triboelectric energy harvester *Smart Mater. Struct.* **27** 015029
[9] Sriphan S and Vittayakorn N 2018 Facile roughness fabrications and their roughness effects on electrical outputs of the triboelectric nanogenerator *Smart Mater. Struct.* **27** 105026
[10] Chen J, Guo H, He X, Liu G, Xi Y, Shi H and Hu C 2016 Enhancing performance of triboelectric nanogenerator by filling high dielectric nanoparticles into sponge PDMS film *ACS Appl. Mater. Interfaces* **8** 736–44
[11] Liu G, Chen J, Tang Q, Feng L, Yang H, Li J, Xi Y, Wang X and Hu C 2018 Wireless electric energy transmission through various isolated solid media based on triboelectric nanogenerator *Adv. Energy Mater.* **8** 1703086
[12] Liu W, Liu G, Jiang D, Wang C, Li W, Guo T, Zhao J, Xi F, Liu W and Zhang C 2018 Interdigitated electrode-based

triboelectric sliding sensor for security monitoring *Adv. Mater. Technol.* **3** 1800189

[13] Xing F, Jie Y, Cao X, Li T and Wang N 2017 Natural triboelectric nanogenerator based on soles for harvesting low-frequency walking energy *Nano Energy* **42** 138–42

[14] Zhang H, Yang Y, Hou T C, Su Y, Hu C and Wang Z L 2013 Triboelectric nanogenerator built inside clothes for self-powered glucose biosensors *Nano Energy* **2** 1019–24

[15] Lee C J, Young A Y, Choi C, Sim H J, Kim S J and Kim Y T 2016 Triboelectric generator for wearable devices fabricated using a casting method *RSC Adv.* **6** 10094

[16] Song Y, Zhang J, Guo H, Chen X, Su Z, Chen H, Cheng X and Zhang H X 2017 All-fabric-based wearable self-charging power cloth *Appl. Phys. Lett.* **111** 073901

[17] Shi M, Zhang J, Chen H, Han M, Shankaregowda S A, Su Z, Meng B, Cheng X and Zhang H X 2016 Self-powered analogue smart skin *ACS Nano* **10** 4083–91

[18] Dhakar L, Pitchappa P, Tay F E H and Lee C K 2016 An intelligent skin based self-powered finger motion sensor integrated with triboelectric nanogenerator *Nano Energy* **19** 532–40

[19] Chen H, Miao L, Su Z, Song Y, Han M, Chen X, Cheng X, Chen D and Zhang H X 2017 Fingertip-inspired electron skin based on triboelectric sliding sensing and porous piezoresistive pressure detection *Nano Energy* **40** 65–72

[20] Lai Y C, Deng J, Liu R, Hsiao Y C, Zhang S L, Peng W, Wu H M, Wang X and Wang Z L 2018 Actively perceiving and responsive soft robots enables by self-powered, highly extensible, and highly sensitive triboelectric proximity- and pressure-sensing skins *Adv. Mater.* **30** 1801114

[21] Wang S, Niu S, Yang J, Lin L and Wang Z L 2014 Quantitative measurements of vibration amplitude using a contact-mode freestanding triboelectric nanogenerator *ACS Nano* **8** 12004–13

[22] Meng B, Tang W, Too Z H, Zhang X, Han M, Liu W and Zhang H X 2013 A transparent single-friction-surface triboelectric generator and self-powered touch sensor *Energy Environ. Sci.* **6** 3235–40

[23] Guo H, Jia X, Liu L, Cao X, Wang N and Wang Z L 2018 Freestanding triboelectric nanogenerator enables noncontact motion-tracking and positioning *ACS Nano* **12** 3461–7

[24] Yang Y *et al* 2018 Liquid-metal-based super stretchable and structure-designable triboelectric nanogenerator for wearable electronics *ACS Nano* **12** 2027–34

[25] Helseth L E 2018 Interdigitated electrodes based on liquid metal encapsulated in elastomer as capacitive sensors and triboelectric nanogenerators *Nano Energy* **50** 266–72

[26] Bartoletti C, Buonanni R, Fantasia L G, Frulla R, Gaggioli W and Sacerdoti G 1998 The design of a proximity inductive sensor *Meas. Sci. Technol.* **9** 1180–90

[27] Helseth L E 2013 Optical fibre spectrometer combined with a magnetic resonance sensor for multiple depth monitoring *Meas. Sci. Technol.* **24** 085605

[28] Mohan S S, Hershenson M, Boyd S P and Lee T H 1999 Simple accurate expressions for planar spiral inductances *IEEE J. Solid-State Circuits* **34** 1419

[29] Wen Z *et al* 2016 Harvesting broad frequency band blue energy by a triboelectric electromagnetic hybrid nanogenerator *ACS Nano* **10** 6526–34

[30] Li X H, Han C B, Zhang L M and Wang Z L 2015 Cylindrical spiral nanogenerator *Nano Res.* **8** 3197–204

[31] Yin X, Liu D, Zhou L, Li X, Zhang C, Cheng P, Guo H, Song W, Wang J and Wang Z L 2019 Structure and dimension effects on the performance of layered triboelectric nanogenerators in contact-separation mode *ACS Nano* **13** 698–705

[32] Schneider F, Fellner T, Wilde J and Wallrabe U 2008 Mechanical properties of silicones for MEMS *J. Micromech. Microeng.* **18** 065008

[33] Dow Corning® 2005 Product information sheet of Sylgard 184 https://consumer.dow.com

[34] Bethe H A and Schwinger J 1943 *Perturbation theory of resonant cavities* NDRC Report Cornell University pp D1–117

[35] Diehl R, Wheatley D M and Castner T G 1996 The electromagnetic modes of a helical resonator *Rev. Sci. Instrum.* **67** 3904–13

[36] Seol M L, Lee S H, Han J W, Kim D, Cho G H and Choi Y K 2015 Impact of contact pressure on output voltage of triboelectric nanogenerator based on deformation of interfacial structures *Nano Energy* **17** 63–71